FACTA UNIVERSITATIS
Ser: **Elec. Energ.** Vol. 25, N° 1, April 2012, pp. 15 - 30
DOI: 10.2298/FUEE1201015A

FIELD EMISSION – BASED MANY-VALUED PROCESSING USING CARBON NANOTUBE CONTROLLED SWITCHES, PART 2: ARCHITECTURE EFFECTUATION

Anas N. Al-Rabadi[1], Marwan S. Mousa[2]

[1]Computer Engineering Department, The University of Jordan, Amman, Jordan
[2]Physics Department, Mu'tah University, Al-Karak, Jordan

Abstract. *A novel field emission Carbon Nanotube (CNT) - based controlled switch is introduced in the second part of the article. For the architecture effectuation of the new CNT field emission – based switching device, four field emission tubes having single CNT as emitters were previously tested and compared to a tungsten-tip tube, and the corresponding Fowler-Nordheim analysis was performed. Measurements conducted with the CNT suggested that mixer current could be 30 times greater if either SWCNT or MWCNT were used in place of metal emitters, increasing the microwave output power by 30 dB. Laser radiation was utilized to increase field emission current from a cathode with a dense field of CNT by a factor of 18. The extension of the new device from the two-valued to the general m-valued case is introduced, and the implementation of many-valued Galois circuits and systems is also shown.*

Key words: *carbon nanotubes, electronic circuits, field emission, many-valued computing, multiplexers, parity checking*

1. INTRODUCTION

Nanotechnology is a new emerging interdisciplinary field of research that covers several important science and technology areas of electronics, chemistry, physics and biology, which analyzes and synthesizes systems in the nano scale (10^{-9} m) such as nanoparticles, nanowires and carbon nanotubes (CNTs) [4,7,8,14,15,17,29,30,33,35,44]. The CNT technology is one of many cutting-edge new technologies within nanotechnology which is showing high efficiency and a very wide range of applications in several various areas in science and engineering [3-7,9,12,14,15,17,24,28,30,35,36,41,44].

Carbon nanotubes have attracted attention in recent years not only for their relatively small dimensions and unique morphologies, but also for their potential implementations in many current and emerging technologies [3-9,12,14,15,17,24,28-30,33,35,36,41,44]. The CNT is made from graphite [8,14,15,17,30,33]. It has been observed that graphite can be formed in nano-scale in three forms: (1) Carbon Nanoball (CNB) (or buckyball) – a

Received October 12, 2011
Corresponding author: Anas N. Al-Rabadi
Computer Engineering Department, The University of Jordan, Amman, Jordan • E-mail: a.alrabadi@ju.edu.jo

molecule consisting of 60 carbon atoms (C_{60}) that are arranged in the form of a soccer ball, (2) Carbon Nanotube (CNT) – a narrow strip of tiny sheet of graphite that comes mainly in two types: (a) multi-wall CNT (MWCNT) where each CNT contains several hollow cylinders of carbon atoms nested inside each other, and (b) single-wall CNT (SWCNT) that is made of just a single layer of carbon atoms, and (3) Carbon Nanocoil (CNC) [8,14,15,17,30,33].

Carbon nanotube, which is a cylindrical sheet of graphite, is geometrically formed in two distinct forms which affect CNT properties: (1) straight CNT in which a CNT is formed as a straight cut from a graphite sheet and rolled into a carbon nanotube, and (2) twisted CNT in which a CNT is formed as a cut at an angle from a graphite sheet and rolled into a carbon nanotube. Fig. 1 shows a carbon nanoball (i.e., buckyball), SWCNT, and Scanning Electron Microscopy (SEM) image of chemical vapor deposition (CVD) grown array of MWCNT towers.

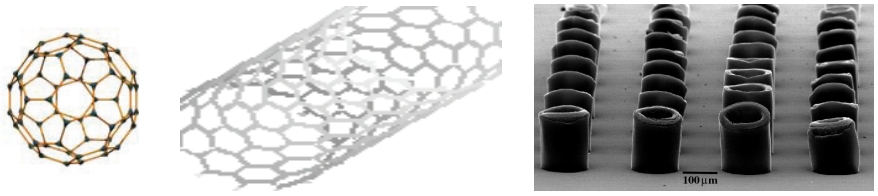

(a) (b) (c)

Fig. 1. Different shapes and formations of CNTs: (a) carbon nanoball (i.e., buckyball), (b) single-wall CNT, and (c) an image from the Scanning Electron Microscopy (SEM) of chemical vapor deposition (CVD) grown array of multi-walled CNT towers.

The emerging CNT technology has been implemented in many new promising applications [3-9,12,14,15,17,24,28-30,33,35,36,41,44]. Recent CNT-based examples of such applications include nanocircuits based on CNTs such as CNT Field Effect Transistors (FETs) that show high potentials for consuming less power and are much faster than the available silicon-based FETs. Other important applications include: (1) TVs that are based on the field emission of CNTs that consume much less power, are thinner and have a much higher resolution than the best plasma-based TVs, (2) nano circuits based on CNTs such as CNT-based FETs that consume less power and are much faster than the available silicon-based FETs, (3) Carbon nanocoils used as inductors in nanofilters and as nanosprings in nano dynamic systems, and (4) CNT rings. The CNT has also potential applications such as in: (1) CNT probes, (2) new composite materials, (3) CNT data storage devices that are capable of storing 10^{15} bytes/cm^2, (4) drug delivery systems, (5) nano lithography, and (6) CNT gears.

Carbon nanotube growth, as observed using (1) Transmission Electron Microscopy (TEM), (2) Atomic Force Microscopy (AFM) and (3) Scanning Electron Microscopy (SEM), requires processes with correct conditions and materials. Currently, several methods for growing various types of CNTs exist [8,14,15,17,30,33]: (1) a big spark between two graphite rods, few millimeters apart, that are wired to a power supply in which a 10^2 Ampere spark between the two rods vaporizes carbon into hot plasma which partially recondenses into the form of CNT, (2) chemical vapor deposition (CVD) of a hot gas such

as methane in which a substrate is placed in an oven, then the oven is heated to approximately 600 degrees Celsius and methane is added slowly; as methane decomposes, it frees carbon atoms that partially re-compose into the form of 0.6-1.2 nm in diameter SWCNTs, and (3) a laser blast of a graphite target in which laser pulses blasts a graphite rod which generates hot carbon gas from which CNT forms.

Despite the fact that CNT has been grown into several forms, CNT use is still limited as compared to other wide spread technologies. This is mainly due to the fact that (1) it is still difficult to exactly control CNT growth into desired forms and (2) CNT growth is still very expensive due to the low yield of CNTs that meet the desired geometrical specifications (cf. the cost property in Table 1). The existing and rapidly growing wide usability of CNTs in several applications is due to the unique structural properties they possess. Table 1 summarizes most of these properties as compared to traditional counterparts [4]. For example, field emission property is used in the recently developed highly efficient CNT-based TVs and is used in new prototype vacuum tube lamps in six colors that are twice as bright as conventional light bulbs, longer-lived and at least ten times more energy-efficient. The properties of current carrying capacity, thermal stability, power consumption and electron scattering qualify the CNT for a very promising future use in highly efficient power transmission. The property of preserving the electron spin will be utilized in using the CNT for reliable spintronics (quantum-based) computations. The size property is very useful for using CNTs as nanowires that would result in decreasing the total size of areas and volumes that are occupied by wires and interconnects in the corresponding integrated circuits. The property of resilience is useful in building circuits and structures that have to maintain stresses without suffering from structural damages. The CNT property of energy band gaps qualifies CNTs to be used in wide applications that require wide range of energy band gaps from the conductor state to the semiconductor state.

Conducted simulations and experiments have shown that photomixing (i.e., optical heterodyning) in laser-assisted field emission could be used as a new microwave or terahertz (THz) source with a multi-octave bandwidth [1,11,13,23-26,29,31,34,37,38]. The field emitter tip used is much smaller than the wavelength of the incident optical radiation so quasi-static conditions require that the electric field of the radiation is superimposed on the applied static field to modulate the height of the energy barrier. Electrons tunnel from the tip into vacuum with a delay τ which is less than 2 fs. Therefore, because the current-voltage characteristics of field emission are extremely nonlinear, it is shown that if two lasers are focused on the tip, the mixer current follows each cycle of the difference frequency of the two lasers from DC up to 500 THz (which is equal to $1/\tau$). It is also shown that the tip will withstand applied static fields as high as 9 V/nm, so that incident laser radiation with comparable field strengths could produce a bright source of microwave or THz radiation. Carbon nanotubes are excellent field emitters [9,10,13,16,19,29,36,38,39,41] and facilitate the miniaturization of electronic devices [3,4,6-9,15,17,24,26-28,30,33,35,36,41]. Furthermore, the kinetic inductance of CNT causes them to be high impedance (approximately 5 kΩ) transmission lines [28], and had shown that this effect can be used for efficient broadband matching to the high impedance that is inherent in field emission. The static and dynamic characterizations of field emitters consisting of a single CNT, both single-walled (SWCNT) and multi-walled (MWCNT) were described [29] and the comparison to a field emitter consisting of an etched single crystal of tungsten was also performed.

Table 1. Properties of Carbon nanotubes.

Property	Single-Walled CNT	By Comparison
Size	0.6 - 1.8 nm in diameter	Electron beam lithography can create lines 50 nm wide and a few nm thick
Density	1.33 – 1.40 g/cm^3	Aluminum has a density of 2.7 g/cm^3
Tensile Strength	$\approx 45 \cdot 10^9$ Pascals	High-strength steel alloys break at $\approx 2 \cdot 10^9$ Pascals
Resilience	Can be bent at large angles and re-straightened without damage	Metals and carbon fibers fracture at grain boundaries
Current Carrying Capacity	$\approx 1 \cdot 10^9$ A/cm^2	Copper wires burn out at $\approx 1 \cdot 10^6$ A/cm^2
Field Emission	Can activate phosphors at 1 – 3 V if electrodes are spaced 1 micron apart	Molybdenum tips require ≈ 50 – 100 V/micrometer with very limited lifetimes
Heat Transmission	≈ 6,000 W/m·K at room temperature	Nearly pure diamond transmits ≈ 3,320 W/m·K
Temperature / Thermal Stability	Stable up to 2,800 C in vacuum and 750 C in air	Metal wires in microchips melt at ≈ 600 – 1,000 C
Cost	≈ 1,500 $/g	Gold sells for ≈ 40 $/g
Preservation of the Quantum Property of Electron Spin	Optimal; Very high	Low in regular conductors
Power Consumption	Very low	Higher in metal wires
Speed	Very high $\geq 1 \cdot 10^{12}$ Hertz nanoscale switch	≥ 1,000 times as fast as processors available today
Electron Scattering (Resistance)	Almost none	Comparatively high
Energy Band Gaps	Easily tunable; Depends on CNT diameter and thus wide range of band gaps can be obtained: ≈ 0 (like a metal), as high as band gap of Silicon, and almost anywhere in between	No other known material can be so easily tuned

This second part of the article introduces a novel CNT field emission – based device that implements an important and fundamental building block in logic synthesis – the controlled switch [2,3,4,7,32,43], and the use of the new device in many-valued computations is also shown for the important case of ternary Galois logic (GF_3), where Fig. 2 illustrates the layout of the introduced CNT-based system design method. Although the many-valued implementation of the new CNT-based controlled switch is demonstrated in this work for the case of GF_3, the implementations and extensions over higher radices of Galois logic and other algebras are similar.

Applications: Nano Systems
Circuits: Nano Circuits
Devices: Nano Devices
Technology: Carbon Nanotube
Physics: Field-Emission
Algebra: Galois Field

Fig. 2. The implementation hierarchy of the introduced CNT-based devices.

The remainder of this article is organized as follows: New CNT field emission-based controlled switch is introduced in Section 2. The implementation of parity-preserving reversible controlled-swap gate using the new CNT-based controlled switch is introduced in Section 3. Several examples of many-valued computations using the new devices are introduced in Section 4. Conclusions and future work are presented in Section 5.

2. New CNT Field Emission – Based Controlled Switch

This Section introduces the basic new device of CNT field emission – based controlled switch, and its extension to the case of many-valued Galois logic.

2.1. Two-to-one controlled switch

Utilizing the previously experimented and observed CNT characterizations and operations that were introduced in Part 1 of this article, Fig. 3 introduces the new CNT field emission – based primitive that realizes the 2-to-1 controlled switch. In Fig. 3, the input control signal that is used to control the electric conduct of the new device is implemented using the imposed electric field intensity (E), or equivalently the work function (Φ) or voltage (V).

The description of the operation of the CNT field emission – based device shown in Fig. 3(b) is as follows: by imposing the control signal of high voltage (HV), the voltage difference between the CNT cathodes and the facing anode is varied. This change will make the CNT cathode with control signal (HV) to be field emitting while the other CNT cathode with the complementary control signal ($\overline{\text{HV}}$) to be without field emission. When the voltage difference is reversed, the CNT cathode with the complementary control signal ($\overline{\text{HV}}$) will be field emitting while the other CNT cathode with the control signal (HV) will be without field emission. Thus, this device implements the functionality of the 2-to-1 controlled switch ($G = ac + b\bar{c}$) shown in Fig. 3(a).

The experimental results show that the distance *d* required between the cathodes and the facing anode must be around 10 mm, or else beam distortion will occur affecting the collected current at the facing anode screen. The equations that relate the electric field intensity (E), work (energy) function (Φ) in Joules (J), distance (d), voltage (V), and the current density (J), are as follows:

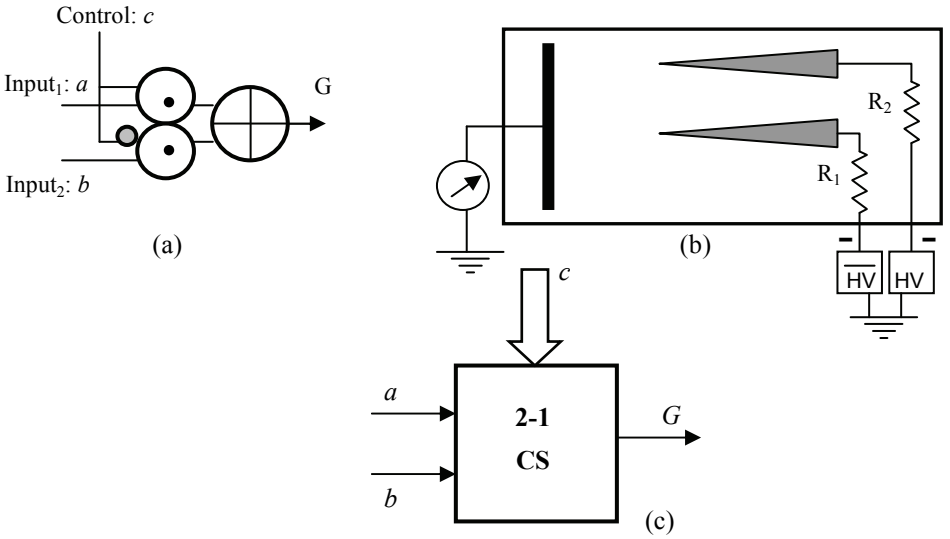

Fig. 3. The CNT - based device implementing the operation of the 2-to-1 controlled switch: (a) the 2-to-1 logic multiplexer ($G = ac + b\bar{c}$), (b) the CNT - based field emission – based 2-to-1 controlled switch, and (c) block diagram for the new 2-to-1 multiplexer.

In this figure, HV is high-voltage source, $\overline{\text{HV}}$ is the complementary (i.e., opposite) high voltage source, and CS is the controlled switch.

$$\Phi = e \cdot V \tag{1}$$

$$V = E \cdot d \tag{2}$$

$$d = V / E \tag{3}$$

$$J = I / (a/\Omega) = I \cdot (\Omega/a) \tag{4}$$

where e is the electron charge $\cong 1.602 \cdot 10^{-19}$ Coulombs (C), a is the tip area, and Ω is the emission angle. Then, the equation which is modeling the current value on the anode screen can be derived as follows:

$$I = \left(\frac{aA}{\Omega d^2} e^{-\frac{Bd}{V}} \right) V^2 \tag{5}$$

From Equation (5), one can clearly observe the corresponding proportionality relation between the current value (I) and the voltage difference (V), proportionality relation between the current value (I) and the tip area (a), and the inverse relation between the current value (I) and the emission angle (Ω), where $A = 1.541 \times 10^{-6}/\Phi$ and $B = 6.831 \times 10^{9}\ \Phi^{3/2}$. The values of the work function are $\Phi = 4.5$ eV for tungsten and for CNT was set to $\Phi = 4.9$ eV for graphene. The typical values which are used for the experiment input control variable of the electric field

intensity (E) is $\geq 3 \cdot 10^9$ V/m, for the distance (d) between the CNT cathode and the facing anode screen is $\cong$ 10 mm, and for the voltage is $V \cong 3 \cdot 10^7$ V.

2.2. The extension to many-to-one controlled switches

Synthesizing many-to-one (i.e., *m*-to-1) CNT field emission – based controlled switches is possible using the fundamental two-to-one CNT field emission – based controlled switch from Fig. 3(b).

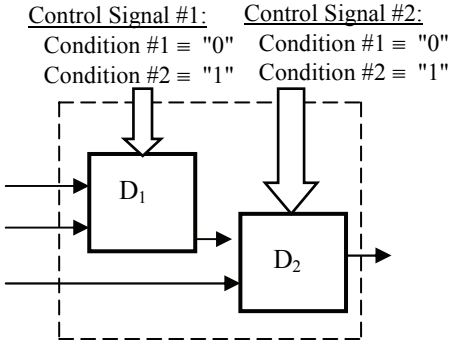

Fig. 4. The 3-to-1 CNT field emission - based controlled switch, where the devices $\{D_1, D_2\}$ are implemented using the CNT-based controlled switch device shown in Fig. 3(b).

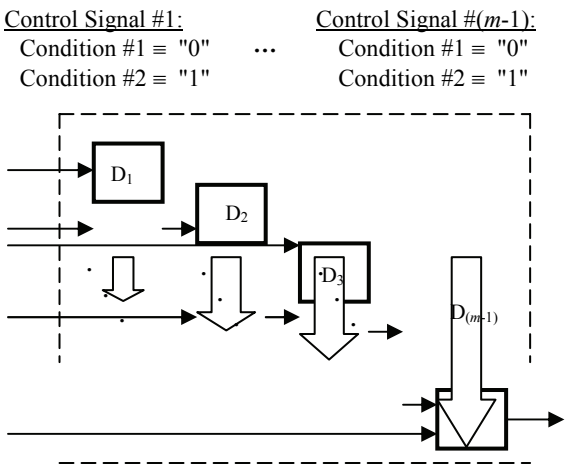

Fig. 5. The realization of an *m*-to-1 controlled switch, where devices $\{D_1,..., D_{(m-1)}\}$ are implemented using the CNT field emission – based controlled switch from Fig. 3(b).

For example, for the 3-valued logic case, one needs two devices from Fig. 3(b) to realize the functionality of three-to-one CNT field emission – based controlled switch. This idea is illustrated in Fig. 4. Note that, in Fig. 4, device D_1 outputs one signal from two input signals and device D_2 outputs one signal from two input signals, thus the total functionality of the device in Fig. 4 is a three-to-one CNT field emission – based controlled switch.

In general, for an *m*-valued logic, one needs (*m*-1) of 2-to-1 controlled switches to realize the function of an *m*-to-1 controlled switch. This is illustrated in Fig. 5.

3. THE IMPLEMENTATION OF PARITY-PRESERVING REVERSIBLE CONTROLLED-SWAP GATE USING THE NEW CNT FIELD EMISSION – BASED CONTROLLED SWITCH

Due to the anticipated approaching failure of Moore's law, quantum computing will play an increasingly important role in building more compact and less power consuming computers. Due to this fact, and because all quantum computer gates (i.e., building blocks) should be reversible (i.e., information lossless) [2], reversible computing will have an increasingly larger existence and utilization in the future design of regular, compact and universal circuits and systems.

Motivations for pursuing the possibility of implementing circuits and systems using reversible logic and quantum computing would include important design objectives such as power minimization, size miniaturization, speed maximization, and added error correction property [2]. For the error correction property, parity checking is one of the oldest and most widely used methods for error detection in digital circuits and systems. It is shown that reversible logic gates having an equal number of inputs and outputs are sufficient for parity preservation if a reversible circuit at each gate is parity-preserving [2,21,42], where parity-preserving reversible logic gates refer to reversible gates for which the parity of the output matches that of the input. The synthesis choice from such gates depends on the circuit design specifications in terms of the number of the used reversible gates, amount of needed "garbage" output which is used only for the purpose of ensuring reversibility, logical complexity, and the number of executed clock cycles.

+	**0**	**1**
0	0	1
1	1	0

(a)

*	**0**	**1**
0	0	0
1	0	1

(b)

+	**0**	**1**	**2**
0	0	1	2
1	1	2	0
2	2	0	1

(c)

*	**0**	**1**	**2**
0	0	0	0
1	0	1	2
2	0	2	1

(d)

Fig. 6. Galois field addition and multiplication tables: (a) $GF_2(+)$, (b) $GF_2(*)$, (c) $GF_3(+)$, and (d) $GF_3(*)$.

Fredkin gate [2] is one of the most fundamental building blocks in reversible and quantum computing, where many propositions have been performed to realize the Fredkin gate in various technologies [2,6] such as optical, electrical, nano mechanical, and quantum. The Fredkin gate belongs to a group of primitives where each primitive represents a fundamental family of logic gates in reversible computing [2] that contain Fredkin-like, Toffoli-like, and Feynman-like gates [2]. It was also shown how to formally generalize the fundamental Fredkin gate to any general *m*-valued Galois logic [2].

In general, and as previously stated, the detection of faults generated in a circuit can be performed using parity-preserving reversible logic gates. Given that reversible gates tend to have the same number of input and output vectors, a sufficient requirement for parity preservation in the course of reversible computation with such gates is that each gate should be parity-preserving, i.e., have the same parity for the input and output vector. The implementation methodologies that are developed is this section and in the following

section are general and are applied in the m-valued Galois radix for $m = p^k$, where p is a prime number and k is a natural number of value $k \geq 1$. Fig. 6 shows important examples of binary and ternary Galois field addition and multiplication tables.

The following definition provides the formal specification for the two-valued parity-preserving reversible logic gate.

Definition 1. For the binary radix of Galois field, let $I = (a; b; c)$ and $O = (P; Q; R)$ be the input and output vectors of a (3, 3) reversible gate, respectively. We call a reversible gate to be a Parity-Preserving Reversible Logic Gate (PPRLG) if the gate satisfies the parity-based equation: $a \oplus b \oplus c = P \oplus Q \oplus R$, where $\oplus$ is the Boolean Exclusive-OR (i.e., XOR) operation which is the GF_2 addition operation.

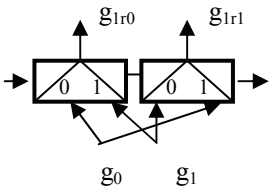

	g_0	g_1	c	g_{1r0}	g_{1r1}	c	
0	0	0	0	0	0	0	**0**
1	0	0	1	0	0	1	**1**
2	0	1	0	0	1	0	**2**
3	0	1	1	1	0	1	**5**
4	1	0	0	1	0	0	**4**
5	1	0	1	0	1	1	**3**
6	1	1	0	1	1	0	**6**
7	1	1	1	1	1	1	**7**

(a)

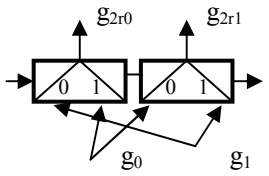

	g_0	g_1	c	g_{2r0}	g_{2r1}	c	
0	0	0	0	0	0	0	**0**
1	0	0	1	0	0	1	**1**
2	0	1	0	1	0	0	**4**
3	0	1	1	0	1	1	**3**
4	1	0	0	0	1	0	**2**
5	1	0	1	1	0	1	**5**
6	1	1	0	1	1	0	**6**
7	1	1	1	1	1	1	**7**

(b)

Fig. 7. Representations for important reversible primitives: (a) reversible GF_2 $Shannon_1$ (i.e., $Fredkin_1$) gate, and (b) reversible GF_2 $Shannon_2$ (i.e., $Fredkin_2$) gate.

Fig. 7 shows two commonly used PPRLGs [2] which are based on the fundamental Fredkin gate (also known as the two-valued reversible Shannon gate [2]). Both of the reversible gates in Fig. 7 are clearly parity-preserving because both of them satisfy the parity-based equation which was shown in Definition 1. While Definition 1 provides the formal specification of binary parity-preserving reversible gates, Definition 2 provides the formal specification of m-valued parity-preserving reversible gates.

Definition 2. A general m-valued Galois Parity-Preserving Reversible Logic Gate (PPRLG) satisfies the equation $a +_m b +_m \ldots +_m c = P +_m Q +_m \ldots +_m R$, where $m = p^k$, p is a prime number, k is a natural number of value $k \geq 1$, and $\{a, b, ..., c\}$ and $\{P, Q, ..., R\}$ are the corresponding input and output vectors of an m-valued $(m + 1, m + 1)$ reversible gate, respectively.

As an example of Definition 2, for the important specific case of the third radix Galois field, let $I = (a; b; c; d)$ and $O = (P; Q; R; L)$ be the input and output vectors of a ternary (4, 4) reversible gate, respectively. A ternary PPRLG is a gate that satisfies the parity-

based GF_3 equation of $a +_3 b +_3 c +_3 d = P +_3 Q +_3 R +_3 L$. For instance, Equation (6) characterizes the operation of the 3-valued Fredkin gate (also known as the 3-valued reversible Shannon gate) [2]:

$$\vec{g} = \begin{bmatrix} {}^2c & {}^0c & {}^1c \\ {}^1c & {}^2c & {}^0c \\ {}^0c & {}^1c & {}^2c \end{bmatrix} \begin{bmatrix} 1 & 0 & 0 \\ 0 & 1 & 0 \\ 0 & 0 & 1 \end{bmatrix} \begin{bmatrix} g_0 \\ g_1 \\ g_2 \end{bmatrix} = \begin{bmatrix} g_{r0} \\ g_{r1} \\ g_{r2} \end{bmatrix} \tag{6}$$

where ${}^ic$ is the 1-Reduced Post Literal which is a single variable function defined as ${}^ic = 1$ if $c = i$ else ${}^ic = 0$ if $c \neq i$ where the variable c can take any value in the set {0,1,2} [2].

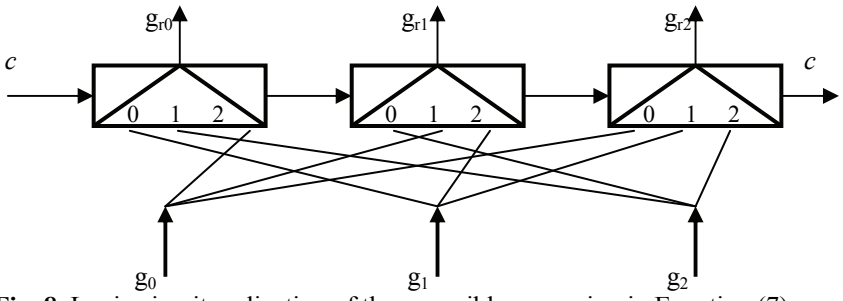

Fig. 8. Logic circuit realization of the reversible expansion in Equation (7).

The corresponding gate that is represented by Equation (6) is reversible given that input c is produced in the output [2] for which a modified form of Equation (6) would be as shown in Equation (7):

$$\vec{g} = \begin{bmatrix} {}^2c & {}^0c & {}^1c & 0 \\ {}^1c & {}^2c & {}^0c & 0 \\ {}^0c & {}^1c & {}^2c & 0 \\ 0 & 0 & 0 & 1 \end{bmatrix} \begin{bmatrix} 1 & 0 & 0 & 0 \\ 0 & 1 & 0 & 0 \\ 0 & 0 & 1 & 0 \\ 0 & 0 & 0 & 1 \end{bmatrix} \begin{bmatrix} g_0 \\ g_1 \\ g_2 \\ c \end{bmatrix} = \begin{bmatrix} g_{r0} \\ g_{r1} \\ g_{r2} \\ c \end{bmatrix} \tag{7}$$

The reversible Shannon expansion in Equation (7) is represented using the 3-to-1 controlled switch as shown in Fig. 8 [2]. Table 2 illustrates the reversibility proof of the 4-input 4-output (i.e., (4, 4)) ternary Fredkin gate shown in Fig. 8 that was formally represented by Equation (7).

Both of the 2-to1 controlled switches in Fig. 7 can be directly implemented using the CNT field emission - based realization that was shown in Fig. 3(b), and the 3-to-1 controlled switch in Fig. 8 can be directly implemented using the 3-to-1 CNT field emission - based realization shown in Fig. 4.

4. MANY-VALUED COMPUTING USING THE NEW CNT-BASED DEVICE

Many-valued computing will be illustrated in this section using the new CNT field emission – based device that was previously developed for the case of ternary radix Galois field (GF_3). Although the demonstration of the use of the new CNT-based controlled switch

is for the case of GF_3, implementations over higher radices of Galois logic follow the same proposed method.

Table 2. The proof of reversibility of the ternary (4,4) gate from Equation (7) and Fig. 8.

Inputs (I)				**Outputs (O)**			
g_0	g_1	g_2	c	g_{r0}	g_{r1}	g_{r2}	c
g_0	g_1	g_2	0	g_1	g_2	g_0	0
g_0	g_1	g_2	1	g_2	g_0	g_1	1
g_0	g_1	g_2	2	g_0	g_1	g_2	2

A controlled switch - based circuit that implements Figs. 6(c) and 6(d) is shown in Fig. 9, where Fig. 9(a) can be implemented using the new two-input single-output CNT field emission – based device from Fig. 3(b).

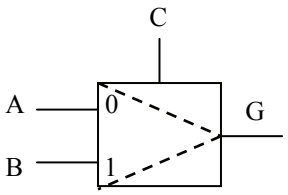

A	B	C	G
a	*b*	0	*a*
a	*b*	1	*b*

(a)

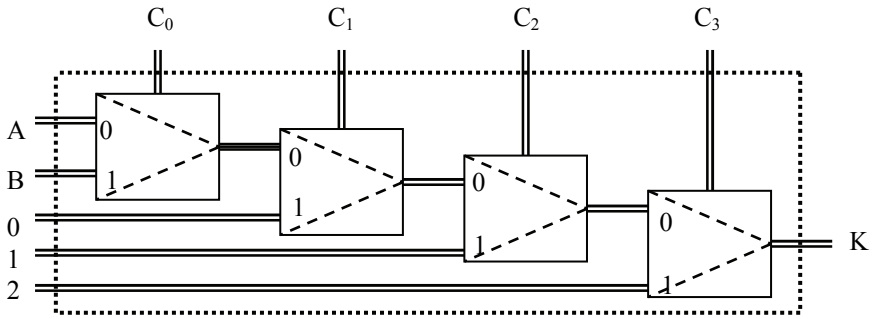

(b)

Fig. 9. The CNT - based implementation of Galois arithmetic operations: (a) controlled switch symbol that can be implemented using the CNT device in Fig. 3(b), and (b) circuit that uses the controlled switch from Fig. 9(a) to implement GF_3 addition and multiplication tables from Figs. 6(c) – 6(d).

The internal nano interconnects in Fig. 9(b) can be implemented using CNTs as well (cf. Fig. 10), where = means a metallic CNT used as a nanowire, especially as the CNT possesses the important properties of small size, high resilience, and very low electron scattering as was shown in Table 1. Several efficient methods for implementing such

interconnects have been reported by growing a SWCNT between two metal catalyst islands such as iron (Fe), cobalt (Co), nickel (Ni), yttrium (Y), or molybdenum (Mo).

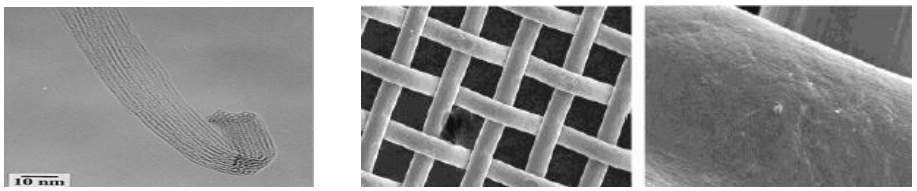

(a) (b)

Fig. 10. The implementation of CNT-based nano interconnects: (a) TEM image of a bundle of SWCNTs catalyzed by Ni/Y mixture, and (b) growing CNT wires on catalysts where CNT meshes are shown on which the metal catalyst is coated.

In Fig. 9(b), the variables {A, B} are two ternary input variables that can take any value from the set {0, 1, 2}, inputs {0, 1, 2} are constant inputs, and inputs C_k (k = 0, 1, 2, 3) are two-valued control variables that take values from the set {0, 1}. Note that Fig. 9(b) implements Figs. 6(c) and 6(d) by using the appropriate values of control variables C_k that select the variable inputs {A, B} and constant inputs {0, 1, 2}, where Table 3 shows an example for the implementation of Figs. 6(c) and 6(d) using Fig. 9(b).
Since m-valued circuits over GF_3 will be synthesized using the addition and multiplication operations from Figs. 6(c) and 6(d), the circuit in Fig. 9(b) can be used in many-valued implementations whenever GF_3 addition and multiplication operations are applied, and the internal nano interconnects can be implemented using metallic CNTs. A simple illustration is presented in Example 1.

Example 1. Let us implement the ternary function $H = X_4X_1 +_3 X_2X_3X_1 +_3 X_2X_3$ using the addition and multiplication operations realized using Fig. 9(b). For instance, the corresponding GF_3 addition and multiplication used in Fig. 11 could be implemented using Table 3 (that specifies input values to Fig. 9(b)) for specifying values to various inputs.

Table 3. An example for the implementation of Figs. 6(c) - 6(d) using Fig. 9(b), where + means GF_3 addition from Fig. 6(c), * means GF_3 multiplication from Fig. 6(d), C_k (+) means that the control variable C_k to implement the ternary addition operation, and C_k (*) means that the control variable C_k to implement the ternary multiplication operation.

A	B	C_0 (+)	C_1 (+)	C_2 (+)	C_3 (+)	C_0 (*)	C_1 (*)	C_2 (*)	C_3 (*)	+	*
0	0	0	0	0	0	0	0	0	0	0	0
0	1	1	0	0	0	0	0	0	0	1	0
0	2	1	0	0	0	0	0	0	0	2	0
1	0	0	0	0	0	1	0	0	0	1	0
1	1	0	0	0	1	0	0	0	0	2	1
1	2	0	1	0	0	1	0	0	0	0	2
2	0	0	0	0	0	1	0	0	0	2	0
2	1	0	1	0	0	0	0	0	0	0	2
2	2	0	0	1	0	0	0	1	0	1	1

The following example shows system-level design of an Arithmetic and Logic Unit (ALU) circuit by illustrating the implementation of a 2-digit multiplier using the newly introduced CNT field emission - based device.

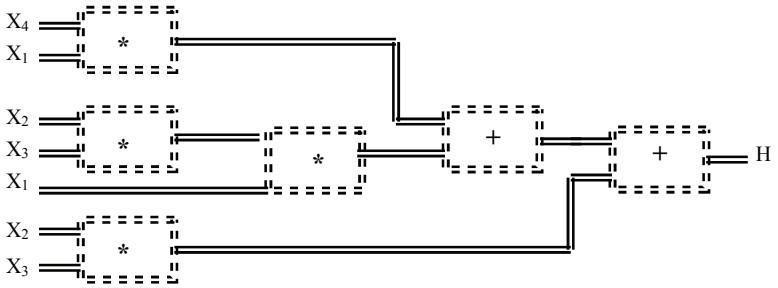

Fig. 11. A GF_3 implementation of $H = X_4X_1 +_3 X_2X_3X_1 +_3 X_2X_3$ using the two-input single-output operators from Figs. 6(c) - 6(d), where Table 3 shows the implementation of Figs. 6(c) - 6(d) using Fig. 9(b), and where = means a metallic CNT used as a nanowire.

Example 2. Let us design a ternary 2-digit multiplier. A 2-digit *m*-valued multiplication is performed utilizing the mod-multiplication operator as follows [2]:

$$\begin{array}{cccccc} & & & B_1 & B_0 \\ & & & \underline{A_1} & \underline{A_0} \\ & & C_{out1} & m_{01} & m_{00} \\ & \underline{C_{out2}} & \underline{m_{11}} & \underline{m_{10}} & \underline{0} \\ C_{out} & S_3 & S_2 & S_1 & S_0 \end{array}$$

Fig. 12 shows the general maps for the ternary multiplication and the output carry (C_{out}) functions, and Fig. 13 shows the corresponding 3-valued circuit realization.

x \ y	0	1	2
0	0	0	0
1	0	1	2
2	0	2	1

(a)

x \ y	0	1	2
0	0	0	0
1	0	0	0
2	0	0	1

(b)

Fig. 12. Ternary 2-digit multiplication: (a) ternary multiply and (b) ternary carry out.

The corresponding GF_3 addition and multiplication operations that are used in Fig. 13 could be implemented using Table 3 that specifies input values to Fig. 9(b) for specifying values to the various inputs. Further implementation of the general *m*-valued *N*-bit full ALU, which is the main functional unit in the microprocessor data path [2,43], that includes the realization of all arithmetic sub-units of addition, subtraction, multiplication and division, and includes the realization of all logic sub-units such as AND, OR and XOR, can be performed from the utilization of the new CNT-based controlled switch device previously introduced by using the same method which was used in the realization of the 2-digit multiplier shown in Fig. 13.

5. CONCLUSIONS AND FUTURE WORK

In this second part of the article, a novel carbon nanotube - based controlled switch is introduced. For the architecture effectuation of the new CNT field emission – based switching device, four field emission tubes having single CNT as the emitters were previously tested, and a tube having a tungsten tip was also used for the corresponding comparison.

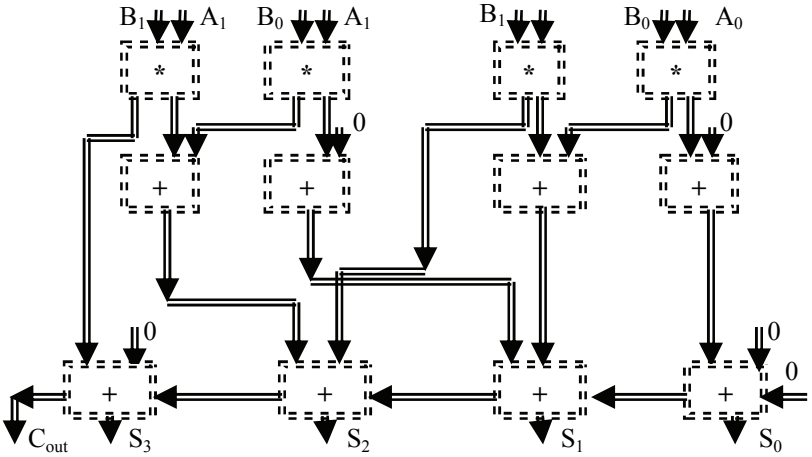

Fig. 13. Logic circuit of a ternary 2-digit multiplier.

The Fowler-Nordheim analysis of the DC current-voltage data gave reasonable values for the local fields at the emitters and the sizes of the emitter sites. Also, two audio-frequency oscillators were used to superimpose sinusoidal signals on the applied static field, thus increasing the DC emitted current. As was previously shown, a single square-wave modulated laser diode of specific power and wavelength focused on each emitter increased the emitted current during each laser pulse with the CNT.

The measurements previously conducted with the CNT suggest that the mixer current could be 30 times greater if either SWCNT or MWCNT were used in place of the metal emitters, which would increase the microwave output power by 30 dB as a considerable improvement. More pertinently, laser radiation was utilized to increase the field emission current from a cathode with a dense field of CNT by a factor of 18, and also was shown that this is not a thermal effect by comparing the corresponding data with the effect of elevated temperatures on the field emission from the used CNT.

The extension of the new two-valued CNT field emission – based device to the general *m*-valued case is introduced, and the general implementations of *m*-valued Galois circuits using the new CNT field emission – based controlled switching devices were also demonstrated. A 2-to-1 controlled switch is a basic building block in "switch logic", where the concept of the *switch logic* is that logic circuits are implemented as combination of switches, rather than a combination of logic gates as in the *gate logic*, which proves to be less-costly in synthesizing a wide variety of logic circuits and systems. Since the controlled switch is of fundamental importance in logic design, the new device can have a wide spectrum of implementations in a wide variety of nano circuits.

Future work will include items such as: (1) the complete fabrication and test of the new CNT field emission – based controlled switching devices, (2) the integrated application of the new nano devices in full system-level computer and electro-mechanical implementations, (3) investigating all of the experimental and fundamental aspects of potential terahertz field ion emission – based controlled switching devices and conduct the comparison with respect to the terahertz field electron emission – based controlled switching devices, (4) investigating all of the experimental and fundamental aspects of thermionic emission (i.e., thermal e^- emission) – based controlled switching devices and conduct the comparisons with respect to field electron emission – based and field ion emission – based controlled switching devices, and (5) investigating new experimental conditions for the distance d between the cathodes and the anode screen to be less than 10 mm without causing any beam distortion and thus without affecting the collected current at the facing anode screen.

REFERENCES

[1] K. Alonso and M. J. Hagmann, "Comparison of three different methods for coupling of microwave and terahertz signals generated by resonant laser-assisted field emission," *Journal of Vacuum Science & Technology B*: *Microelec. Nanometer Structures*, 19(1): 68-71, 2001.

[2] A. N. Al-Rabadi, *Reversible Logic Synthesis*: *From Fundamentals to Quantum Computing*, Springer-Verlag, New York, 2004.

[3] A. N. Al-Rabadi, "Carbon nano tube (CNT) circuits," In Proceedings of the Post-Binary Ultra Large Scale Integration (ULSI) Workshop, Toronto, Canada: 2004, pp. 44-49.

[4] A. N. Al-Rabadi, "Carbon nano tube (CNT) multiplexers for multiple-valued computing," *Facta Universitatis – Electronics and Energetics*, vol. 20, no. 2, pp. 175 -186, 2007.

[5] A. N. Al-Rabadi, "New dimensions in non-classical neural computing, Part I: three-dimensionality, invertibility, and reversibility," *Int. J. Intell. Comp. Cyber.*, Emerald, vol. 2, no. 2, pp. 348-385, 2009.

[6] A. N. Al-Rabadi, "New dimensions in non-classical neural computing, Part II: quantum, nano, and optical," *Int. J. Intell. Comp. Cyber.*, Emerald, vol. 2, no. 3, pp. 513-573, 2009.

[7] A. N. Al-Rabadi, *Carbon NanoTube* (*CNT*) *Multiplexers, Circuits, and Actuators*, United States Patent and Trademark Office, Patent No. US 7,508,039 B2, U.S.A., 24 March 2009.

[8] G. Amaratunga, "Watching the nanotube," *IEEE Spectrum*, pp. 28-32, 2003.

[9] J.-M. Bonard, J.-P. Salvetat, T. Stöckli, L. Forro, and A. Chatelain, "Field emission from carbon nanotubes: perspectives for applications and clues to the emission mechanism," *Applied Physics A*: *Materials Science & Processing*, 69(3): 245-254, 1999.

[10] J.-M. Bonard, K. A. Dean, B. F. Coll, and C. Klinke, "Field emission of individual carbon nanotubes in the scanning electron microscope," *Phy. Rev. Let.*, 89(19): 197602-1:4, 2002.

[11] M. Brugat, M. S. Mousa, E. P. Sheshin, and M. J. Hagmann, "Measurement of field emission current variations caused by an amplitude modulated laser," *Mat. Sci. Eng. A*, 327(1): 7-15, 2002.

[12] P. J. Burke, "Luttinger liquid theory as a model of the gigahertz electrical properties of carbon nanotubes," *IEEE Transactions on Nanotechnology*, 1(3): 129-144, 2002.

[13] H.-F. Cheng, Y.-S. Hsieh, Y.-C. Chen, and I.-N. Lin, "Laser irradiation effect on electron field emission properties of carbon nanotubes," *Diam. and Related Mat.*, 13(4-8):1004-1007, 2004.

[14] P. G. Collins and P. Avouris, "Nanotubes for electronics," *Scientific American*, pp. 62-69, 2000.

[15] P. G. Collins, M. S. Arnold, and P. Avouris, "Engineering carbon nanotubes and nanotube circuits using electrical breakdown," *Science*, vol. 292, 2001.

[16] K. A. Dean and B. R. Chalamala, "Current saturation mechanisms in carbon nanotube field emitters," *Applied Physics Letters*, 76(3): 375-377, 2000.

[17] V. Derycke, R. Martel, J. Appenzeller, and P. Avouris, "Carbon nanotube inter- and intramolecular logic gates," *Nano Letters*, vol. 0, no. 0, A - D, 2001.

[18] R. H. Fowler and L. W. Nordheim, "Electron emission in intense electric fields," *Proc. Royal Society A*: *Mathematical, Physical and Engineering Sciences*, 119(781): 137-181, 1928.

[19] T. Fujieda, K. Hidaka, M. Hayashibara, T. Kamino, Y. Ose, H. Abe, T. Shimizu, and H. Tokumoto, "Direct observation of field emission sites in a single multiwalled carbon nanotube by Lorenz microscopy," *Japanese Journal of Applied Physics*, 44(4A): 1661-1664, 2005.

[20] R. Gomer, "Field emission and field ionization," *American Vacuum Society Classics*, American Institute of Physics (AIP), 1993.

[21] M. Haghparast and K. Navi, "Design of a novel fault tolerant reversible full adder for nanotechnology based systems", *World Applied Sciences J.*, vol. 3, no.1, pp. 114-118, 2008.

[22] M. J. Hagmann, "Mechanism for resonance in the interaction of tunneling particles with modulation quanta," *Journal of Applied Physics*, 78(1): 25-29, 1995.

[23] M. J. Hagmann, "Stable and efficient numerical method for solving the Schrödinger equation to determine the response of tunneling electrons to a laser pulse," *International Journal of Quantum Chemistry*, 70(4-5): 703-710, 1998.

[24] M. J. Hagmann, "Simulations of photon-assisted field emission: their significance in basic science and device applications," *Ultramicroscopy*, 79(1-4): 115-124, 1999.

[25] M. J. Hagmann, "Single-photon and multiphoton processes causing resonance in the transmission of electrons by a single potential barrier in a radiation field," *International Journal of Quantum Chemistry*, 75(4-5): 417-427, 1999.

[26] M. J. Hagmann, "Wide-band-tunable photomixers using resonant laser-assisted field emission," *Applied Physics Letters*, 83(1): 1-2, 2003.

[27] M. J. Hagmann, M. S. Mousa, M. Brugat, E. P. Sheshin, and A. S. Baturin, "Large-signal and small-signal electronic equivalent circuits for a field electron emitter," *Surface and Interface Analysis*, 36(5-6): 402-406, 2004.

[28] M. J. Hagmann, "Isolated carbon nanotubes as high-impedance transmission lines for microwave through terahertz frequencies," *IEEE Transactions on Nanotechnology*, 4(2): 289-296, 2005.

[29] M. J. Hagmann and M. S. Mousa, "Time-dependent response of field emission by single carbon nanotubes," *Jordan Journal of Physics*, vol. 1, no. 1, pp. 1-7, 2008.

[30] J. R. Heath and M. A. Ratner, "Molecular electronics," *Physics Today*, pp. 43-49, 2003.

[31] P. Hommelhoff, Y. Sortais, A. Aghajani-Talesh, and M. A. Kasevich, "Field emission tip as a nanometer source of free electron femtosecond pulses," *Phy. Rev. Let.*, 96(7): 077401-1:4, 2006.

[32] R. C. Jaeger, *Microelectronic Circuit Design*, McGraw-Hill, New York, 1997.

[33] J. Jiao, E. Einarsson, D. W. Tuggle, L. Love, J. Prado, and G. M. Coia, "High-yield synthesis of carbon coils on tungsten substrates and their behavior in the presence of an electric field," *Journal of Materials Research*, vol. 18, no. 11, pp. 2580-2587, 2003.

[34] M. J. G. Lee and E. S. Robins, "Thermal relaxation of a laser illuminated field emitter," *Journal of Applied Physics*, 65(4): 1699-1706, 1989.

[35] K. Likharev, "Hybrid semiconductor-molecular nanoelectronics," *Ind. Phy.*, pp. 20-23, 2003.

[36] Y. Liu and S. Fan, "Field emission properties of carbon nanotubes grown on silicon nanowire arrays," *Solid State Communications*, 133(2): 131-134, 2005.

[37] A. Mayer and J.-P. Vigneron, "Quantum-mechanical simulations of photon-stimulated field emission by transfer matrices and Green's functions," *Phy. Rev. B*, 62(23): 16138-16145, 2000.

[38] A. Mayer, N. M. Miskovsky, and P. H. Cutler, "Photon-stimulated field emission from semiconducting (10, 0) and metallic (5, 5) carbon nanotubes," *Phy. Rev. B*, 65(19): 195416-1:6, 2002.

[39] A. Mayer, N. M. Miskovsky, and P. H. Cutler, "Three-dimensional simulations of field emission through an oscillating barrier from a (10, 0) carbon nanotube," *Journal of Vacuum Science & Technology B*, 21(1): 395-399, 2003.

[40] L. W. Nordheim, "The effect of the image force on the emission and reflexion of electrons by metals," *Proc. Royal Society A*: *Math., Phy. Eng. Sciences*, 121(788): 626-639, 1928.

[41] A. N. Obraztsov, I. Pavlovsky, A. P. Volkov, E. D. Obraztsova, A. L. Chuvilin, and V. L. Kuznetsov, "Aligned carbon nanotube films for cold cathode applications," *Journal of Vacuum Science & Technology B*, 18(2): 1059-1063, 2000.

[42] B. Parhami, "Fault-tolerant reversible circuits," In Proc. 40th Asilomar Conf. Signals, Systems and Computers, Pacific Grove, CA: 2006, pp. 1726-1729.

[43] D. A. Patterson and J. L. Hennessy, *Computer Organization and Design*: *The Hardware / Software Interface*, Morgan-Kaufmann, 2008.

[44] R. Tarkiainen, M. Ahlskog, J. Penttila, L. Roschier, P. Hakonen, M. Paalanen, and E. Sonin, "Multiwalled carbon nanotube: Luttinger versus Fermi liquid," *Phy. Rev. B*, 64(19): 195412-1:4, 2001.